Conformational Preadjustment in Aqueous Claisen Rearrangement Revealed by SITS-QM/MM MD Simulations

ARTICLE *in* THE JOURNAL OF PHYSICAL CHEMISTRY B · APRIL 2015

Impact Factor: 3.3 · DOI: 10.1021/jp511057f · Source: PubMed

4 AUTHORS:

Jun Zhang
Peking University
6 PUBLICATIONS **1** CITATION
SEE PROFILE

Yi Isaac Yang
University of Lugano
8 PUBLICATIONS **4** CITATIONS
SEE PROFILE

Lijiang Yang
Peking University
39 PUBLICATIONS **814** CITATIONS
SEE PROFILE

Yi Qin Gao
Peking University
98 PUBLICATIONS **1,996** CITATIONS
SEE PROFILE

THE JOURNAL OF PHYSICAL CHEMISTRY B

Article

pubs.acs.org/JPCB

Conformational Preadjustment in Aqueous Claisen Rearrangement Revealed by SITS-QM/MM MD Simulations

Jun Zhang,[†,‡] Yi Isaac Yang,[†] Lijiang Yang,[†,‡] and Yi Qin Gao*[,†,‡]

[†]Institute of Theoretical and Computational Chemistry, College of Chemistry and Molecular Engineering, and [‡]Biodynamic Optical Imaging Center, Peking University, Beijing 100871, China

Supporting Information

ABSTRACT: An efficient sampling method was implemented in QM/MM hybrid molecular simulations to study aliphatic Claisen rearrangement in aqueous solutions. On the basis of the computational results, the necessary conformational adjustment to trap the reactant into a favorable compact conformation specifically in water was observed. The conformational equilibrium was shown to be important to the elucidation of the "water-acceleration" effect of Claisen rearrangement. Thus, a two-step process of aqueous Claisen rearrangement was proposed. It was similar to the pseudodiaxial−pseudodiequatorial conformational equilibrium observed in the enzymatic reaction of chorismate acid but with explicit inclusion of the solvent coordinates to explain the solvation effects. Polarization was found to occur during the reactant conformational transition. A solvent with high cohesive energy density (CED) like water was suggested to accommodate compact conformers better, thus facilitating the following reaction by concentrating the real "active" reactant. The substituent effects also manifested, leading to varied conformational distributions of different substituted allyl vinyl ethers (AVEs). The application of the enhanced sampling method allowed a systematic analysis of thermodynamic information without loss of solvent coordinates. These data showed the conformational transition of AVEs was an entropy-driving process which was sensitive to the substituent, and enthalpy played an important role in the solvation effect on the conformational equilibrium.

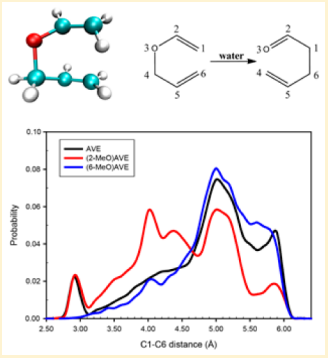

INTRODUCTION

MC and MD simulations have been helping chemists perceive chemical processes at the atomic level and understand more deeply the underlying mechanisms of chemical reactions including solvation effects.[1] In all Monte Carlo (MC) or molecular dynamics (MD) simulation studies, one key element is the accuracy of the potential energy functions used to describe intermolecular interactions. Molecular mechanics (MM) force fields have prevailed in treating large systems where solutes or proteins merely undergo conformational changes without alteration in electronic structures.[2] MM force fields certainly have their limitations, particularly for problems where the response of substrate electrons becomes important, such as processes involving induced dipoles or even rupture and formation of chemical bonds. A reasonable approach is to combine quantum mechanical (QM) and molecular mechanical methods in MC and MD simulations, which will get at a good trade-off between computational accuracy and expenses.[3,4] In such a hybrid QM/MM potential, solute or the reactant is normally treated with quantum mechanics, whereas the rest of the system, normally the environment, is approximated molecular-mechanically.

Specifically, to investigate solvent effects in aliphatic Claisen rearrangement, the reorganization of electrons of the substrate may occur during the process of both conformational adjustment and the sigmatropic shifts.[5,6] Therefore, a rigorous quantum mechanical treatment of the entire system would be ideal in determining the potential energy surface. However, this approach would be too time-consuming to be practical due to the immense size and complexity of the system. Instead, molecular mechanical force fields have built up a reliable database providing sufficient potential functions to frame ordinary solvents and biological complexes.

Over the past two decades, a lot of computational efforts including the *ab initio* continuum method and hybrid MC/MD have been paid to Claisen rearrangement.[7−11] Some of these applications have shown to be successful in explaining the substituent effects and evaluating the interactions between solvents and solute molecules during the "transition process" which usually entailed several predefined reaction coordinates, and highlighted the key role of dipole−dipole interactions.[8,9] However, due to limitations of computational power, these simulations all started from a prerefined "proper" structure, and the so-called transition state (TS) was defined according to the intrinsic reaction coordinates (IRCs) instead of a real, statistically defined transition state.[7,8] It would be important to investigate to what extent the thermodynamic properties obtained from this energy landscape based on predefined reaction coordinates yield the molecular mechanism of the reaction and how good the sampling over the space orthogonal to the reaction coordinate was. Particularly, it is noticeable that previous theoretical approaches to solvent effects in Claisen

Received: November 4, 2014
Revised: April 2, 2015
Published: April 7, 2015

DOI: 10.1021/jp511057f
J. Phys. Chem. B 2015, 119, 5518−5530

rearrangement appeared to underestimate the importance of hydrophobicity[12] and the entropy penalty due to the computational difficulty in accounting for the solvent coordinates.[10,13] Besides, dipole−dipole interactions (including induced dipoles) should be considered throughout the reaction, although little attention has been paid to this aspect when conformational changes of the reactant were dealt with.

Given that normal MD or MC is not efficient enough to cover the relevant phase space practically, it would be difficult to achieve a full picture of the conformational space without using enhanced sampling methods, let alone the transition pathways, thus entailing predefined reaction coordinates or collective variables.[14,15] These issues above are expected to be alleviated when appropriate sampling methods are applied in QM/MM MC/MD simulations. Aimed at improving sampling efficiency and avoiding manipulating the real energy landscape, several enhanced sampling methods were integrated within MC/MD including REMD,[8] metadynamics,[16] umbrella sampling,[17] ITS,[18] etc.

In this paper, we recruited the selective integrated tempering sampling method (SITS)[19] in the hybrid QM/MM MD simulation to establish/propose a new toolkit free of IRCs or collective variables (CVs) for investigations over environment-sensitive chemical processes. This combination enabled us to acquire more accurate information from the subsystem of interest and efficiently obtain convergent thermodynamics for a selectively "excited" region without strongly perturbing the environment. We used this method to simulate Claisen rearrangement and tried to explore the mechanism of aqueous acceleration effects, where the hydrophobic effects and electronic responses were found to bear significant impact on the conformation distribution of the reactant.

In fact, Chandler and Hynes et al. emphasized the importance of solvent coordinates in their studies of chemical reactions involving conformational changes.[20,21] Schwartz et al. revealed a vibrational promoting effect of the condensed phase on chemical reactions.[22] However, earlier studies paid limited attention to the conformational distributions of AVEs in solutions,[8,23] despite that some studies tried to examine the solvent effects on conformational transitions along certain inner reaction coordinates of chorismate acid.[24−26] In contrast, SITS enabled us to search the conformational ensemble of the reactant in the solvation environment rather than focus only on several predefined structures.[25] In this way, the impact of the solvent on the solute conformation could be investigated systematically and thoroughly.

From the observed conformational equilibrium, we defined the compact reactant which was the reactive candidate for the following chemical reaction. Also, the compact conformers drastically accumulated in aqueous solutions. This result was not completely unexpected, echoed by clues from both experimental work and natural enzymatic paradigms.[27] Some previous simulation results indicated that the enzymatic acceleration of chorismate rearrangement might be caused by a higher proportion of the proper configured substrate in water than in methanol.[3,5,26,28] Different from the hydrophilic enzymatic substrate, we showed that, in terms of small hydrophobic molecules, the conformational transition was influenced not only by enthalpy but also by entropy, and might be subjected to the hydrophobic effect. Our findings are in good agreement with experiments[28,29] which tended to accredit the enhancement of the reactivity of AVE in water partly to the hydrophobic effect. Thus, our results might provide more insight into the water-acceleration effect[29,30] of Claisen rearrangement. The conclusion that water could accommodate some hydrophobic solutes might also apply for other "in-water" reactions.[30,31] From the perspective of green chemistry, our findings supported that hydrophobicity of reactants, which usually led to poor dissolvability, would sometimes turn into advantages; thus, more considerations of using water to perform chemical reactions involving hydrophobic reactants like AVEs could be practical.

METHODS

For a hybrid QM/MM system, the total Hamiltonian is divided into three terms in the form of eq 1,[3] where $\mathbf{H}_{QM}$ stands for the energy of QM-treated regions, $\mathbf{H}_{MM}$ for the energy of MM-treated regions, $\mathbf{H}_{QM/MM}$ for the interaction between the two regions, and $\mathbf{H}_t$ for the total energy of the entire system.

$$\hat{\mathbf{H}}_t = \hat{\mathbf{H}}_{QM} + \hat{\mathbf{H}}_{QM/MM} + \hat{\mathbf{H}}_{MM} \quad (1)$$

In our modeling system, the solute alone is treated with QM, so there are no covalent bonds that cross the QM−MM boundary, and the overpolarization on the boundary[3] is no more a concern here.

There are abundant options for QM methods such as AM1, PM3, DFTB, DFT, etc.[32] Generally, according to the complexity of the systems and the specific issue under research, one can choose the most suitable and practical method, if not most accurate. Here in this article we decide on SCC-DFTB[33,34] to quantify the potential energy of the solute considering that this method generally ensures better accuracy than AM1, performs reliably in polar systems, and is computationally extremely efficient compared to the first-principle methods.[35] The current DFTB parameter library works quite well for peptide and organic compound structures and conformation energies, the geometries of hydrogen-bonded systems are well reproduced, and also include dispersion energies.[33] In recent years, SCC-DFTB has been extensively benchmarked (see also Table S2, Supporting Information) and widely utilized in research involving organic compounds, biomolecules, and materials, giving reliable results.[36−38]

The self-consistent charge density functional tight-binding (SCC-DFTB) scheme, developed by Seifert and Elstner et al., is a semiempirical method which is based on the density functional theory (DFT).[33,35,39] This method expands the DFT total energy functional to the second order, with respect to the electron density fluctuations $\delta\rho$ with a given reference density ρ_0. Atom-centered point charges given by the Mulliken population analysis ($\Delta q_\alpha = q_\alpha - q^0_\alpha$ where q_α = electronic charge on atom α, q^0_α = electronic charge on an isolated atom α) are used to depict the second-order term in the density fluctuations. Hence, the approximate total energy is given by eq 2:[40]

$$E_{total} = \sum_{i}^{occ.} \sum_{\mu\nu} c^{\nu}_{\mu} c^{i}_{\nu} \mathbf{H}_{\mu\nu}[\rho_0] + \frac{1}{2} \sum_{\alpha\beta} \Delta q_\alpha \Delta q_\beta \gamma_{\alpha\beta} + E_{rep}[\rho_0] \quad (2)$$

Elements in the Hamiltonian matrix elements $\mathbf{H}_{\mu\nu}$ are calculated with generalized-gradient-approximation DFT (DFT-GGA) with a minimal basis of atomic-like wave functions. The wave function expansion coefficients c^{ν}_{μ} in eq 2 can be obtained by iteratively solving a set of Kohn−Sham equations, which results from applying the variation principle to eq 2. The second term in eq 2 represents the long-range

DOI: 10.1021/jp511057f
J. Phys. Chem. B 2015, 119, 5518−5530

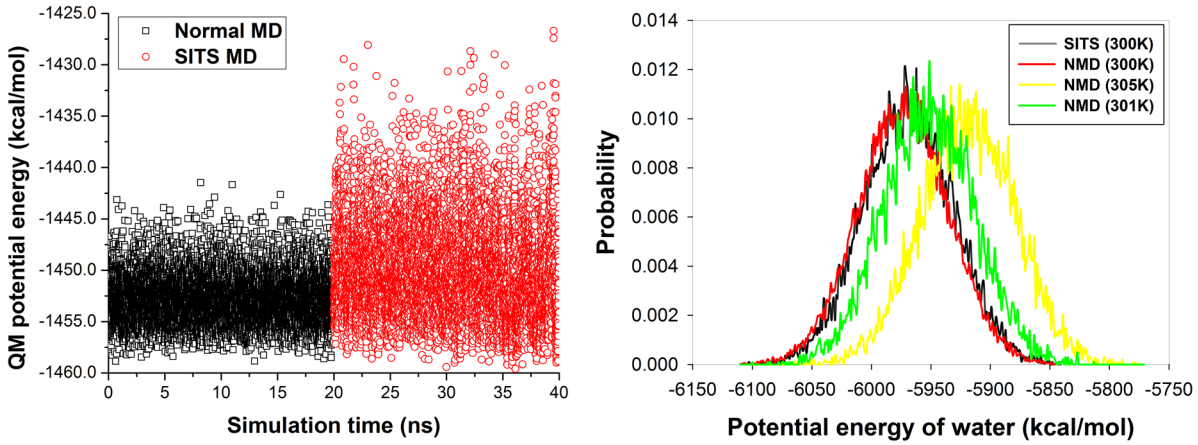

Figure 1. Comparison of the sampling efficiency between normal MD (NMD) and SITS MD. (left) Black and red hollow dots represent the QM-energy profiles along NMD and SITS MD trajectories with the same time length, respectively. (right) Potential energy distributions of solvent (water) in the AVE−water system under different thermostats are collected. The energy distributions of water in NMD and SITS MD at the same temperature 300 K (red and black lines) are almost identical. However, when raising the temperature up to 305 K, a stark difference in the energy distribution of the solvent arises.

Coulomb interactions between the atomic point charges and does not exclude the self-interaction contributions of individual atoms. The third term is the repulsion energy, which is further approximately reduced as a sum of two-center terms $U[\mathbf{R}_{\alpha\beta}]$ by eq 3. The two-body interaction potential $U(r)$ is calculated by subtracting the DFT total energy from the SCC-DFTB electronic energy as a function of the bond distance $r = R_{\alpha\beta}$.

$$E_{\mathrm{rep}}[\rho_0] = \sum_{\alpha<\beta} U[\mathbf{R}_{\alpha\beta}] \tag{3}$$

Then, we implemented the original SITS algorithm[18,41] for MM potentials in QM/MM calculations. In order to focus the computation on enhancing sampling of the phase space of interest (here the QM-treated region) and meanwhile keep the environment (MM-treated) at the target temperature, a rescaled potential surface as a function of temperature is introduced by eq 4, and the effective biased force can be figured out with eq 5,[18] in which U_{eff} is the effective potential and F_{eff} the effective force; E_{MM}, E_{QM}, and $E_{\mathrm{QM/MM}}$ stand for the energy of the MM region, QM region, and QM/MM interaction, respectively; β_0 and β_k represent Boltzmann factors at temperature T_0 (namely, the target temperature) and T_k; n_k's are weighting factors obtained through an iterative procedure;[42] and r denotes the coordinate by convention.

$$U_{\mathrm{eff}} = E_{\mathrm{MM}} - \frac{1}{\beta_0} \ln \sum_k n_k \mathrm{e}^{-\beta_k (E_{\mathrm{QM}} + E_{\mathrm{QM/MM}})} \tag{4}$$

$$F_{\mathrm{eff}} = -\frac{\partial U_{\mathrm{eff}}}{\partial r} = \frac{\sum_k \beta_k n_k \mathrm{e}^{-\beta_k U}}{\beta_0 \sum_k n_k \mathrm{e}^{-\beta_k U}} F_{\mathrm{QM}} \tag{5}$$

SIMULATION DETAILS

For MD of aqueous solutions, the water solvent box was applied with periodic boundary conditions. In the system, the reactant in the aliphatic Claisen rearrangement as the only solute, which could be parent ally vinyl ether (AVE), substituted (2-MeO)AVE or (*Z*-6-MeO)AVE (abbreviated as (6-MeO)AVE for convenience in the remaining text), was treated with SCC-DFTB, whereas the solvent molecules were treated with a molecular mechanical force field by adopting the SPCE water model.[43] Force field parameters for all the solutes were fitted in the general AMBER force field[44] after geometry optimization using Gaussian 09 (revision A.02),[45] and assigned with RESP-A1A charges[46] by the RED software package.[47,48] The concentration of the aqueous solution approximated to 0.09 mol/kg (lower than the saturation limit at room temperature). For nonaqueous solvents, the simulation details were attached in the Supporting Information.

The final series of MD simulations were executed on the AMBER10 package.[32] The QM/MM generalized Born implementation uses the model described by Pellegrini and Field,[49] while regular QM/MM Ewald support is based on the work of Nam et al.[50] with QM/MM PME support based on the work of Walker et al.[51] SCC-DFTB support was written by Gustavo Seabra, Ross Walker, and Adrian Roitberg.[52] The maximum number of SCC iterations in each round of DFTB calculation was set to be 70. SHAKE[53] was used to constrain all covalent bonds involving hydrogens. The MD step was 2 fs. All MD simulations were executed under the isothermal−isobaric (NTP) ensemble, at 1 atm and 300 K (if not stated specifically). The QM region was sampled by SITS. The temperatures used in eq 4 ranged from 220 to 628 K with 50 sampling intervals uniformly chosen for all the MD systems.

Each solution system was first subjected to 500 steps of steepest descent energy minimization, followed by 2000 steps of conjugate gradient optimization. Then, 50 ps MD was performed to heat the system up to 300 K, followed by another 50 ps MD to relax. To equilibrate the system to the appropriate volume, the pressure of the system was adjusted to 1 atm by the Berendsen weak-coupling algorithm[54] with relaxation time constants of 0.2 ps under another 2 ns long normal MD. After an equilibration step, a short (∼10 ns) but prerequisite simulation for determining a proper $[n_k]$ series for subsequent SITS-MD was performed using standard QM/MM MD simulation. Then, SITS simulation was carried out using n_k's determined earlier, and all the MD simulations ran 100 ns long (for IL solutions, we elongated the simulation time to over 150 ns). The first 10 ns of the hybrid SITS-MD was discarded before the data analysis. Thermodynamic properties were

DOI: 10.1021/jp511057f
J. Phys. Chem. B 2015, 119, 5518−5530

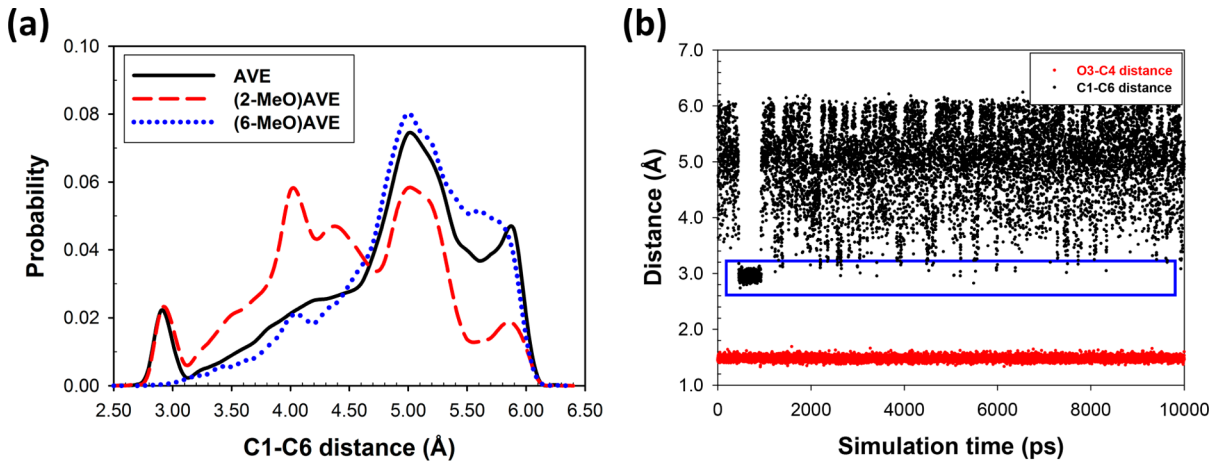

Figure 2. (a) Distribution functions of the distance between C1 and C6 atoms of different reactants in aqueous solution. The black solid, red dashed, and blue dotted lines correspond to the parent, 2-methoxyl substituted, and 6-methoxyl substituted AVEs, respectively. Conformations with a C1−C6 distance shorter than 3.25 Å (which can be reached by the right-bottoms of the Gaussian-like peaks) were defined to be compact, and the others were defined to be extended. (b) Exemplary profiles of C1−C6 distance (black dots) and O3−C4 distance (red dots) along a 10 ns trajectory. A wide range of C1−C6 distance can be adopted; the blue-colored inset box circles out the frames containing compact conformers. O3 and C4 atoms are separated by a normal C−O single bond length with tiny fluctuation. On average, there were tens of transitions between different conformations per nanosecond driven by SITS.

Scheme 1. Aliphatic Claisen Rearrangement of Allyl Vinyl Ether (AVE, Left), (2-MeO)AVE (Middle), and (6-MeO)AVE (Right)[a]

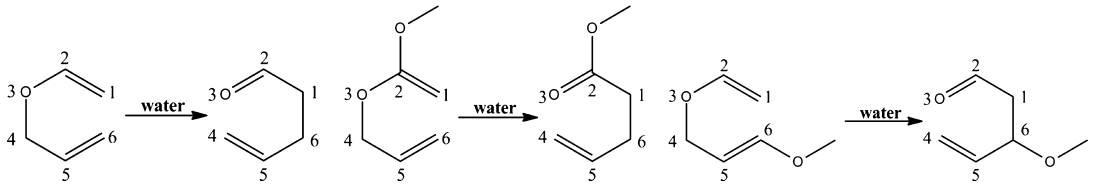

[a]Numeral tags at each atom are the corresponding atom indices.

retrieved at 300 K (if not stated specially) from SITS through a standard reweighting procedure in reference of eqs 6 and 7,[18] where A and A_i stand for the mean value and the ith observed value of the desired thermal properties, w_i for weighting factor, β for Boltzmann factor, and U_i for the energy of the state.

$$\langle A \rangle = \frac{\sum_i w_i A_i}{\sum_i w_i} \tag{6}$$

$$w_i = \frac{e^{-\beta U_i}}{\sum_i e^{-\beta U_i}} \tag{7}$$

RESULTS

I. Convergence and Sampling Efficiency of SITS. SITS achieved a quick convergence within 2 ns for each solvent−solute system. The n_k's in eqs 4 and 5 were updated every 0.2 ps, and it became steady after the first 1 ns, indicating an efficient tempering sampling in the rest of the trajectory.

Referring to the potential energy distributions of the parent solute (AVE) extracted from traditional MD and SITS MD trajectories both of 2 ns in length, respectively (Figure 1), the simulation using the SITS algorithm covered a wide energy space encompassing that of the normal MD. Such a comparison at the same cost of computation assured us of a faster convergence for calculating thermodynamic properties assisted by SITS. Meanwhile, in order to maintain a weakly perturbed environment, the solvent should stay close to room temperature distributions when SITS was applied. To test this assumption, the sampling of the MM region (the solvent) was examined (Figure 2). In fact, water molecules in SITS-MD behaved similarly to those in the normal MD under 300 K thermostat. Thus, SITS enabled sampling with higher efficiency, reweighting the data to the target temperature, and finally quantifying desired thermodynamic properties.

Despite that properties of the solute which were reweighted to a temperature excessively deviating from 300 K might lose the physical sense because the solvent environment was set under the isothermal condition (namely, 300 K), still, performing the reweighting process in the neighboring range of the preset MD temperature was reasonable and acceptable, given that the thermostat was fluctuating all the time. To elaborate on this point, normal MD trajectories under 305, 301, and 299 K were shot additionally. Actually, the potential energy distribution of water ranging from 299 to 301 K only changed slightly and the major peak region remained substantially overlapped (Figure 1, right, and Figure S4, Supporting Information).

II. Definition of the Compact Conformation. By convention, the main chain atoms on the reactant were numbered from C1 to C6 including an O3 heteroatom (Scheme 1). C1 and C6 were the bond-forming sites, while the O3−C4 bond was expected to break in the pericyclic reaction.[55]

In aqueous solution, reactants can be divided into two distinctive conformational categories. One was the compact

DOI: 10.1021/jp511057f
J. Phys. Chem. B 2015, 119, 5518−5530

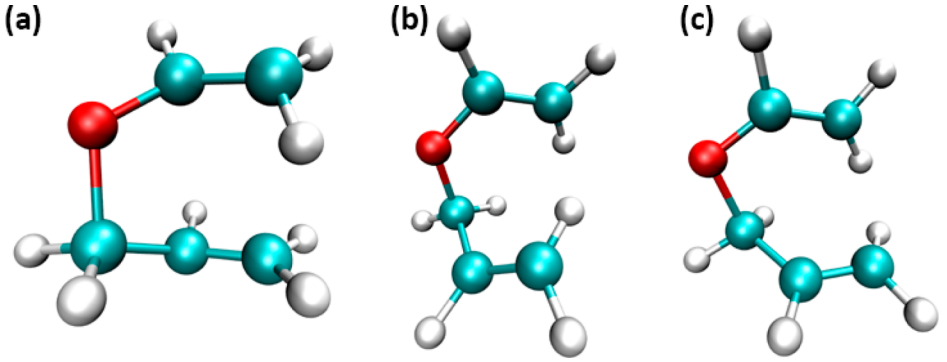

Figure 3. Typical structure for the compact conformation defined in the QM/MM study, including quasi-6-member ring (a), quasi-7-member ring (b), and quasi-8-member ring (c). Carbon, oxygen, and hydrogen atoms are rendered in cyan, red, and white colors, respectively.

conformation characterized by a rather short distance between the C1 atom and the C6 atom, and the other with relatively extended C1−C6 distances (Figure 2a). The compact structures were similar to those found in earlier studies of AVE by Jorgensen et al., which was closed to the local minimum along the reaction path.[11]

The compact conformation was well-defined structurally. Besides the short C1−C6 distance, the compact reactant molecule is rigid with most of the intramolecular dihedrals and bond angles showing small fluctuations. The shape of the molecule resembles either a 6-member ring, consistent with the putative structure of the activated complex (Figure 3a), or a quasi-7/8-member ring with one or two more terminal hydrogen atom(s) involved (Figure 3b and c). Of all the compact conformations, C1−C6 distances centered at 3.0 Å with a slight fluctuation. A conformation with a C1−C6 distance shorter than 2.5 Å was not observed. Compared with the result from previous KIEs indicating that C1−C6 distances of transition states with different substituted AVEs were shorter than 2.4 Å, it could be concluded that all the changes that occurred in the simulation did not involve chemical transitions; hence, they can be regarded merely as conformational changes. Besides, a normal oxygen−carbon single bond length (∼1.45 Å, Figure 2b) adopted by O3−C4 in both conformations was also consistent with this inference. On the other hand, in light of the QM-potential energy (SCF energy) analysis of AVE and (2-MeO)AVE (Table 1), the compact conformers exhibited a slightly lower potential energy than extended ones.

It is intriguing and important to examine the conformational distribution of AVEs in other solvents. We collected the conformation profile of AVE in several commonly used organic solvents, including protonated and dipolar methanol, non-protonated dipolar DMSO, and nonprotonated weakly dipolar toluene. SITS enabled us to efficiently search the conformational space of the solute in all of these solvents.[56] Interestingly, the conformational distribution in these three very different organic solvents turned out to be very similar (Figure 4a), all characterized by the absence of the peak in the window of compact conformation. Moreover, we calculated the QM-energy difference of AVE during conformational changes in these three solvents, but no evidence was found that the intramolecular energy of the compact conformation was lower than that of the extended one in these contexts (Table S3, Supporting Information).

Table 1. Potential Energy of the QM Region (Units: kcal/mol)[a]

	AVE	(2-MeO)AVE	(6-MeO)AVE
compact conformation	−1454.3(0.9)	−1871.2(0.5)	−1862.0(0.5)
extended conformation	−1452.5(0.1)	−1870.4(0.7)	−1862.0(0.1)

[a]Numbers in parentheses are the standard deviations (SDs) of all the block average values for QM potential energies in each solute−water system. For all the tables below, numbers in parentheses are the standard deviations of corresponding block average values, if not stated specifically.

III. Charge Redistribution and Substituent Effects. As mentioned above, in water, transformation from extended to compact structures slightly reduced the energy of the solute itself. From the perspective of molecular mechanics, this phenomenon could only be accredited to the changes of bond angles, dihedrals, and interatom distances. However, resorting to quantum mechanics, it is interesting to find that electrons in AVE actually responded to the conformational changes on top of all the molecular mechanical changes. Potential bond-forming sites (namely, C1 and C6) together with their terminal hydrogen atoms (Figure 5) become polarized in compact conformers. As shown in Figure 5, the charge depletion chart exhibited a small but non-negligible redistribution of electrons across the molecule, especially on the potential reactive sites, during the conformational transition. This QM result highlighted the importance of distinguishing the compact conformation from its extended counterpart in terms of electron density distribution.

The charge redistribution for AVE was also checked in other solvents, but no significant polarization was observed (Figure S5, Supporting Information). It might follow that, in water, the intramolecular multipoles of the solute were readjusted to stabilize the compact conformers and optimize both the intramolecular interactions and the interaction with water. However, in methanol and other organic solvents, conformation transitions of the solute were not sensitive to the environment, and such kind of electron response was greatly weakened.

To obtain more details on the polarization due to the conformational change, population analyses of the other two different substituents were also conducted. Figure 5 shows that the 2-methyoxyl substituent has a charge redistribution similar to parent AVE, whereas 6-methoxyl-AVE is hardly polarized. This result signifies that the polarization of the reactant during the conformational change is sensitive to the substituents. In this case, the substituent effect interplays with the solvent

DOI: 10.1021/jp511057f
J. Phys. Chem. B 2015, 119, 5518−5530

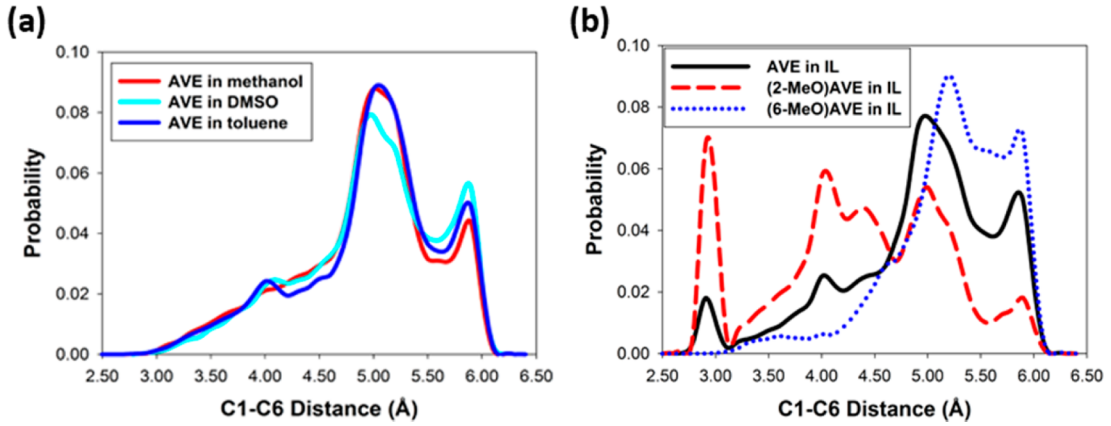

Figure 4. (a) Conformational distributions of AVE in methanol (red line), DMSO (cyan line), and toluene (blue line). (b) Conformational distributions of AVE (black solid line), (2-MeO)AVE (red dashed line), and (6-MeO)AVE (blue dotted line) in ionic liquid.

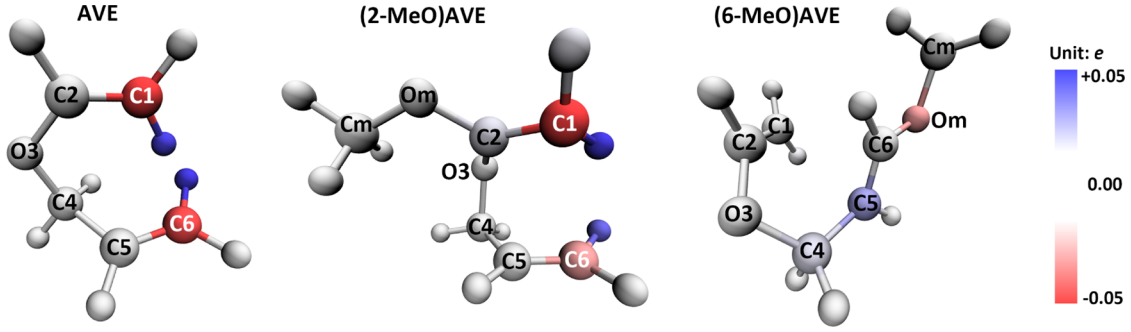

Figure 5. Charge polarization chart of AVE (left), (2-MeO)AVE (middle), and (6-MeO)AVE (right) in aqueous solutions. Within the spheres are the atomic name and index (Cm and Om represent the carbon and oxygen atoms at the methyl group). Coloring of the spheres represents the charge differences by subtracting the average Mulliken population of the compact conformation with that of the extended conformation. Red colored regions denote atoms gaining more electron density, whereas blue colored regions suffer a depletion of electrons, after transforming from extended to compact conformation.

Table 2. Thermodynamics of the Conformational Equilibrium at 300 K in Water

	AVE	(2-MeO)AVE	(6-MeO)AVE
P_c	0.060(0.003)[a]	0.088(0.002)	0.015(0.004)
K_{conf}	0.064(0.003)	0.097(0.002)	0.015(0.004)
ΔG_{conf}[b] (kcal·mol^{-1})	1.64 (0.02)	1.39(0.01)	2.5(0.1)
ΔS_{conf} (cal·mol^{-1}·K^{-1})	−8.8(0.7)	−4.9(1.4)	−9.6(0.6)
ΔH_{conf} (kcal·mol^{-1})	−0.9(0.4)	−0.1(0.5)	−0.4(0.1)
ΔG_{conf}[c] (kcal·mol^{-1})	1.7	1.4	2.5
ΔV_{conf}[d] (cm^3·mol^{-1})	−23(7)	−14(7)	−2(6)

[a]Numbers in parentheses are corresponding standard errors. See more details in the Supporting Information. [b]ΔG_{conf} derived from eq 10. [c]ΔG_{conf} recovered from ΔH_{conf} and ΔS_{conf} in Table 2 by applying eq 14, at T = 300 K. Uncertainties are not shown. [d]ΔV_{conf} stands for the partial volume change of the solute during transitions from extended to compact conformation.

effects. It can be inferred that substituents which could stabilize the polarization in a given solvent would promote the transition from the extended to compact conformation.

IV. Thermodynamics of the Conformational Transition in Solutions. *1. Distribution of Conformations in Water.* After the system reached equilibrium, the probabilistic distribution of different conformers according to their C1−C6 distance was calculated. Both AVE and 2-methoxyl-AVE exhibited a sharp peak near where the C1−C6 distance was slightly less than 3.0 Å, but this peak was absent in (6-MeO)AVE. Notice that the peaks arose from where C1−C6 was slightly more than 2.5 Å and then declined to minima at about 3.25 Å, and this C1−C6 distance window perfectly matches our definition of the compact conformation. The area below the first peak in the distribution curve was calculated to give the population of compact conformers in the system. In the region of larger C1−C6 distance (>3.3 Å), the shapes of the three curves resembled each other. They represent the population of random extended conformations, which led to similar probabilistic distributions; except for (2-MeO)AVE, there was a relatively higher peak at ∼4.0 Å than the other two reactants. The main disparity of these curves lay in the area below the first peak, or rather the window of compact conformation, indicating a strong substituent effect was bearing on the propensity of the solute to adopt compact structures.

2. Conformational Equilibrium Constant in Water. To further test such a substituent effect, the equilibrium constant at 300 K, K_{conf}, was calculated to characterize the conformational

DOI: 10.1021/jp511057f
J. Phys. Chem. B 2015, 119, 5518−5530

transition. The probability of adopting the compact conformation, P_c, was easily obtained by integrating the probability density over the compact conformation window (r < 3.25 Å) conforming to eq 8. Then, P_c is rephrased into K_{conf} using eq 9. The compact conformation was more favorable if the K_{conf} value was larger. K_{conf}'s for three different systems are listed in Table 2. (2-MeO)AVE displays the largest K_{conf} value due to a much higher "peak-tail" around 3.2 Å than parent AVE despite that the peak value of (2-MeO)AVE was almost the same as that of AVE. Again, K_{conf} of (6-MeO)AVE was significantly smaller than the other two K_{conf}'s.

$$P_c = \int^{3.25\text{Å}} P(r)\, dr \tag{8}$$

$$K_{conf} = \frac{P_c}{1 - P_c} \tag{9}$$

The convergence of the data set for conformational distribution was evaluated by the standard deviation of the block average of P_c. Given that the conformational transition is a relatively fast process, SITS actually ensures a fairly satisfactory convergence of the conformational distribution (see SI Text II and Table S1, Supporting Information).

3. Thermodynamics of Conformational Change in Water. Next, the van't Hoff isothermal equation (eq 10) was applied to calculate the Gibbs free energy, $\Delta G_{conf}(T)$, and it was a function of temperature.

$$\Delta G_{conf}(T) = G_{cp} - G_{ex} = -RT \ln K_{conf}(T) \tag{10}$$

On top of ΔG_{conf}, more thermodynamic details were required to depict the conformational transition process. In principle, one SITS MD simulation simultaneously integrated the configurational distributions of the selected region over a wide range of temperatures. This feature allowed us to retrieve thermodynamics of the solute at different temperatures.

The weighting factor of the SITS simulation was calculated at four other temperature scales near 300 K (299, 299.5, 300.5, and 301 K, respectively) first.[57,58] Then, the corresponding $K_{conf}(T)$ and Gibbs free-energy changes $\Delta G_{conf}(T)$ were updated in the same procedure as mentioned above.

Starting from the series of Gibbs free energy at small temperature intervals, the classic Gibbs−Helmholtz equation (eq 11) was applicable to plot out the enthalpy change in between different conformers. The conformational changes occurring here were under constant pressure, so eq 11 applied to both G_{cp} and G_{ex} and then eq 11 can be rewritten as eq 12:

$$\frac{\partial}{\partial T}\left(\frac{G}{T}\right)_p = -\frac{H}{T^2} \tag{11}$$

$$\frac{\partial}{\partial T}\left(\frac{\Delta G_{conf}}{T}\right)_p = -\frac{\Delta H_{conf}}{T^2} \tag{12}$$

$\Delta H_{conf}(T_0)$ is then obtained as the local slope at $1/T_0$ of the $(\Delta G_{conf}/T)-1/T$ curve. Gibbs free energy data from 299 to 301 K were used to acquire enthalpy information at 300 K. A scattering data plot of $\Delta G_{conf}/T-1/T$ was delivered, and it was further fitted into a linear form (Figures S1 and S2, Supporting Information). The results are shown in Table 2. In all three systems, ΔH_{conf} was negative. Thus, the compact conformation of parent and substituted AVEs is enthalpically favorable in aqueous solutions.

Next, the entropy of conformational change was obtained using eq 13. The procedure of deriving the entropy change is similar to that of enthalpy analysis, and Figure S1 (Supporting Information) shows a paradigm.

$$\left(\frac{\partial \Delta G_{conf}}{\partial T}\right)_p = -\Delta S_{conf} \tag{13}$$

It can be seen from Table 2 that the aqueous system with parent AVE suffered a large entropy loss as a result of the conformational transition, ca. −8.8 cal·mol^{-1}·K^{-1}. For 6-methoxyl-AVE, the entropy loss was even larger. In contrast, the transition from the extended to compact conformation is associated with a much smaller entropy loss, ca. −4.9 cal·mol^{-1}·K^{-1} for 2-methoxyl-AVE in water solution. Herein, the substituent effect was found to influence entropy changes as well. This result was in accordance with the kinetic isotope effect (KIE) experiment which recorded a large acceleration effect of 2-methoxyl substitution,[29] indicating the conformational entropy penalty might be critical in Claisen rearrangement.

The negative conformational entropy changes were in accordance with the total activated entropy of Claisen rearrangement which was known to be negative. It is likely to originate from the "frozen" intramolecular degrees of freedom in the compact structure. The total activation entropy of Claisen rearrangement in the gas phase (heated at ∼450 K) was ca. −7.8 cal·mol^{-1}·K^{-1}.[59] Thus, the entropy change during the conformational change was already comparable to $\Delta^{\ddagger}S$, suggesting the entropy penalty was majorly overcome during the conformational adjustment rather than the bond-forming/breaking process. Our results could explain why in enzymes the activation entropy was significantly reduced in contrast to the uncatalyzed Claisen rearrangement.[27] Besides, we found that different substituents influenced the entropy changes, leading to a varied population of compact conformers in water.

It is noteworthy that, with ΔH_{conf} and ΔS_{conf} we derived following the above procedure, ΔG_{conf} can be recovered by applying eq 14, thus justifying the self-consistency of this method (Table 2). In addition, we examined the robustness of such a methodology for deriving ΔH_{conf} and ΔS_{conf} from ΔG_{conf} (see SI Text III, Supporting Information).

$$\Delta G_{conf} = \Delta H_{conf} - T\Delta S_{conf} \tag{14}$$

Following exactly the same procedure, we collected the thermodynamic properties of AVE during conformational changes in methanol, DMSO, and toluene (Table 3). In all the solvents we used, forming the compact conformation was an entropy-losing process, which was consistent with the physical intuition. In reference of ΔG_{conf} in water, the data

Table 3. Conformational Equilibrium of AVE at 300 K in Nonaqueous Solvents

solvent	methanol	DMSO	toluene	ionic liquid
$\Delta\Delta G_{conf}$[a] (kcal·mol^{-1})	1.2	1.3	1.2	0.2
$\Delta\Delta S_{conf}$ (cal·mol^{-1}·K^{-1})	0.1	−0.4	0.2	−1.3
$\Delta\Delta H_{conf}$ (kcal·mol^{-1})	1.1	1.1	1.1	−0.2
ΔV_{conf}[b] (cm^3·mol^{-1})	3(8)	2(6)	7(6)	−10(8)

[a] $\Delta\Delta G_{conf} = \Delta G_{conf}$ (in nonaqueous solvent) − ΔG_{conf} (in water); the same definition of "ΔΔ" goes for other thermodynamic properties. Statistical errors were not shown. [b] Defined in the same way as in Table 2.

DOI: 10.1021/jp511057f
J. Phys. Chem. B 2015, 119, 5518−5530

showed that ΔG_{conf} in these solvents rose by ca. 1.2 kcal/mol. Noteworthy, after dissecting $\Delta\Delta G_{conf}$ into an entropy term and an enthalpy term, we found it was the $\Delta\Delta H_{conf}$ that accounted for most of the free energy increase.

4. Volume Change of the Solution and the Cohesive Energy Penalty. On the basis of a negative activated volume (ca. -10 $cm^3 \cdot mol^{-1}$) in Claisen rearrangement,[60] inference had been put forward that in water the reactant state could be more destabilized than the transition state due to the large cohesive pressure (or cohesive energy density), although little computational work exists to test this idea. The cavity volume which the solute created might correlate with the extent of destabilization. Since it is difficult to quantify the size of the "cavity", the volume change of the entire solution (ΔV_{conf}), containing 1 mol of solutes (at a certain concentration) which underwent conformation transitions, is used instead. The total volume change of the system under constant pressure could be represented by eq 15, where $V_{compact}$ and $V_{extended}$ stand for the total volume of the systems with compact and extended solute, respectively. Note that, by this definition, ΔV_{conf} is dependent on the concentration of the solution. For the three solutions discussed here, the concentration of each approximates to be 0.09 $mol \cdot kg^{-1}$.

$$\Delta V_{conf} = V_{compact} - V_{extended} \quad (15)$$

For AVE and (2-MeO)AVE, the observed volume of the aqueous solution decreased significantly when compact structures formed (Table 2). The extent of such conformational volume change was even greater than that of the activated volume; hence, it should not be negligible for computations in aqueous solutions.

It is known that the hydrophobic effect could cause nonpolar organic molecules to aggregate and macromolecules to collapse.[61] Inspired by the negative ΔV_{conf}, we supposed that the hydrophobic effect/water contributed a lot to stabilizing the compact conformers. To verify this hypothesis, the energy compensation caused by "shrinking" of the solution cavity (ΔU_{cav}) was estimated using eq 16, where c stood for the cohesive pressure of the solvent.

$$\Delta U_{cav} = c \cdot \Delta V_{conf} \quad (16)$$

The cohesive pressure of water at near room temperature is about 0.55 $kcal/cm^3$; thus, with $\Delta V_{conf} \approx -14$ cm^3/mol (as with 2-methoxyl-AVE in water), the energy preference for water to accommodate compact conformers was up to about 8 kcal/mol. This would be a rather large contribution to stabilizing the aqueous solution containing compact conformers apart from the intramolecular interaction, although this value was overestimated given that the size of the vacuum cavity should be smaller than the total volume change of the solution.

In contrast to water, common organic solvents such as methanol, toluene, DMSO, etc., exhibited a much smaller cohesive energy density; thus, the effect caused by a negative volume change of the condensed phase was negligible. In fact, the volume of these organic solutions did not decrease in response to the formation of the compact conformation (Table 3). This result is a reasonable explanation of the accumulation of the compact conformation in water compared to other solvents we have tested. Besides, due to the weaker polarity of these organic solvents, the dipole−dipole and dipole−mulitpole interactions could be weakened to a great extent compared to aqueous solution. Thus, taking compact structures was no longer favorable in terms of enthalpy.

5. Conformational Preadjustment of AVEs in Ionic Liquid. Inspired by the above results and analyses, we suggested that, if a solvent exhibited strong intermolecular interactions including those due to the hydrogen bond network or electrostatic attraction, the population of the compact conformation of AVE would be enhanced. Ionic liquids serve as good examples, since they are among the few solvents known to exhibit a larger CED than water. Another series of SITS-QM/MM MD simulations were executed using the three solutes aforementioned, with TiF−BF_4 ion pairs as the surroundings. After the same methodology was used for the conformation analysis of AVEs in ionic liquid, we found that the peak representing the compact conformation resurrected for AVE and (2-MeO)AVE (Figure 4b). For (2-MeO)AVE, the compact conformers were even more populous in ionic liquid than in water. This observation solidifies our proposal that the hydrophobic interactions and the large cohesive energy of water (and IL) are the key factors that accumulate the compact conformation of AVEs in aqueous solutions (and in IL).

Again, we found no significant population of the compact conformation in the (6-MeO)AVE system, indicating the substituent effect was present similarly to that in water. Additionally, as observed in water, AVE and (2-MeO)AVE were polarized during the conformational transitions in ionic liquid (Figure 4), which might lead to better solute−solvent interaction modes. Meanwhile, the volume of the ionic liquid system decreased as the compact conformation was adopted by the solute. These phenomena led to more enthalpy compensation for the formation of the compact conformation (see Table S3, Supporting Information), provided that ionic liquid has a larger CED than water. However, it remains elusive how the substituents influenced the shrinkage of water and IL. Actually, the parent AVE induced a smaller volume decrease of IL, whereas (2-MeO)AVE in IL experienced a larger volume shrinkage when adopting the compact structure than in water, consistent with the observed more favorable enthalpy compensation and larger population of the compact conformation (Table S4, Supporting Information, and Figure 4b).

DISCUSSION

As the earliest recorded [3,3] sigmatropic reaction, the Claisen rearrangement of allyl vinyl ethers (AVEs) has played an important role both in synthetic strategy for carbon−carbon bond formation and in the primary metabolism process. Great efforts have been exerted in obtaining details of the mechanism, catalysis, and solvent effects of this pericyclic reaction. Decades ago, a couple of substituted AVE substrates for Claisen rearrangement were demonstrated to bear appreciable solvent effects which challenged the traditional view that Claisen rearrangement underwent an isopolar transition state. Gao et al. calculated the polarity of the transition states for different substituted AVEs in several solvents, and concluded that the polarity of the activated complex differed with different substitutions, and that dipole−dipole interaction between the reactant and solvent was critical in stabilizing the TS.[8] Given that the observed acceleration of both parent and substituted AVEs did not correlate with the increasing polarity of solvents in a simple manner, there should be other factors involved.[12] Since the 1980s, several studies have reported that some organic reactions were substantially promoted in aqueous solutions whereas the reactants even could not dissolve in water, including the famous Diels−Alder reaction, Mukaiyama reaction, and Claisen rearrangement.[30] Many postulations were

DOI: 10.1021/jp511057f
J. Phys. Chem. B 2015, 119, 5518−5530

brought up to explain such an unexpected phenomenon. In terms of Claisen rearrangement, many argued the hydrogen-donating capacity of water molecules, analogous to Lewis acid catalysis, would destabilize the TS;[11,62] some added that the huge polarity of water might contribute to stabilizing the TS,[8] while others insisted the hydrophobic effects dominate on grounds of the well-known negative $\Delta^{\ddagger}V$ and $\Delta^{\ddagger}S$ in this pericyclic process.[12,63] However, all of the above perspectives were mainly focused on the transition path, with limited explicit considerations of the underlying solvent effects on the conformational space of reactants. Two decades ago, researchers turned their attention to the conformation of chorismate acid during the study of enzymatic catalysis of Claisen rearrangement. With NMR experiments and high-accuracy computational methods, two metastable structures of chorismate acid were discovered in water.[64] An equilibrium was proposed to describe the transition between the two typical structures. The solvent effects over this equilibrium were also examined, mainly from the energetic perspective.[26]

I. Intermediate State. Claisen rearrangement is a pericyclic reaction. Undoubtedly, this reaction requires a proper 6-member ring conformation prior to electronic arrangement, or the concerted bond breaking and forming event. Thus, the compact conformation as we defined must be involved. In other words, the reaction has to go through the compact conformation to further evolve to the transition state. The compact conformation defined above is more or less reminiscent of the conformational equilibirum in the studies on chorismate acid, in which a conformation close to the T.S. was necessary for the ensuing chemical reaction.[65−67] Therefore, the compact conformers could be an important "intermediate state" along the overall reaction path. We have observed the ensemble distributions of both the compact conformers and the extended ones of AVEs in several solvents, while the population of the compact conformation varies drastically in different contexts.

This simple argument enables us to add more details to the aliphatic Claisen rearrangement, and generalize the scheme proposed for chorismate acid. A conformational equilibrium is established before the subsequent chemical event takes place (Scheme 2). The total reaction barrier for aliphatic Claisen rearrangement is no less than 30 kcal·mol^{-1}.[68] In contrast to the high barrier of the rate-limiting step of electronic rearrangement, the transition between different conformers suffers a fairly low energy barrier (less than 4 kcal/mol) and is fast enough to reach an approximate but rational equilibrium. This scheme would assist us to gain deeper insight of the solvent effects on this aged chemical reaction.

Scheme 2. Conformational Preadjustment of Aqueous Claisen Arrangement[a]

$$R_{extended} \underset{\Delta G_{conf.}}{\overset{K_{conf.}}{\rightleftharpoons}} R_{compact} \xrightarrow{k_{ele.}} T.S. \longrightarrow P$$

[a] $R_{extended}$ stands for extended conformer, and $R_{compact}$, for compact conformer. T.S. is short for transition state complex, and P, for product. K_{conf} and ΔG_{conf} represent the conformational equilibrium constant and Gibbs free energy, respectively, while k_{ele} denotes the rate coefficient of the following chemical bond rearrangement.

As a first-order kinetic mechanism, the previous kinetic equation (eq 17) for Claisen rearrangement is rewritten into eq 18, where $[c]_0$ and $[c]_{cp}$ stand for the concentration of the reactant and the compact conformers based on the conformational distribution; k_{ele}, $k_{overall}$, and $r_{overall}$ denote the first-order rate constant of electronic rearrangement and the overall reaction and the overall reaction rate, respectively. This scheme seems similar to the proposed conformational equilibrium for chorismate acid by Jorgensen et al., but our definition of compact or extended conformers was based on the sampling of molecular configurations, instead of local structures representing stationary points at the potential energy surface.[26]

According to our results that the conformation transition can be much faster than the chemical bond forming/breaking event, the primary overall rate constant comes as a product of the conformational equilibrium constant and the rate constant of electronic rearrangement. Several simulations have been conducted to reveal factors impacting on the stability of the transition state and the rate constant k_{ele}, lacking detailed discussions on the substituent and solvent effects on K_{conf}.[7,8] Through our effort, K_{conf} was calculated for AVE in several solutions. Meanwhile, we have calculated the k_{ele} in water using an enhanced sampling method for trajectories.[19,69] Starting from the compact conformation and according to eq 19, the overall rate coefficient from enhanced sampling of the trajectory was $k_{overall} = 1.4 \times 10^{-4}$ s^{-1} for AVE in water, which is in good agreement with the experimental value.[29,70−72]

$$r_{overall} = k_{overall}[c]_0 \tag{17}$$

$$r_{overall} = k_{ele}[c]_{cp} = \frac{K_{conf}}{K_{conf} + 1} k_{ele}[c]_0 \tag{18}$$

$$k_{overall} = \frac{K_{conf}}{K_{conf} + 1} k_{ele} \tag{19}$$

II. Solvation and Substituent Effects on K_{conf} of AVEs. According to the transition-state theory, the activated free energy of Claisen rearrangement can be changed into another form by taking eq 20 into account:

$$\Delta G^{\ddagger} = \Delta G_{conf} + \Delta G_{ele}^{\ddagger} \tag{20}$$

Theoretical studies revealed that the preference of the pseudodiaxial conformation in water compared to methanol or the gas phase was attributable to the hydrogen-bonding pattern and hence to the energy.[24,26] However, from the perspective of structure ensemble, ΔG_{conf} for AVEs cannot be addressed by the potential energy changes only. Adopting the compact conformation means losing intramolecular entropy or creating a penalty to free energy. Therefore, without compensations from either enthalpy or entropy of the solvent, this process would be unfavorable.

However, from the free-energy data fitted with the Gibbs−Helmhotz equation, the enthalpy of the entire aqueous system is found to decrease slightly in response to the formation of compact conformers. According to our analysis, such advantageous energy tendency for the compact conformation arises partly from intramolecular polarization. Noticeably, our simulation shows that the conformational equilibrium constant is also significantly affected by the substituents. Earlier research has demonstrated substituents will alter the dipolar properties during the bond-forming/breaking event.[9] Moreover, here we show that, during conformational changes, different substituents also lead to varied patterns of electronic polarization. It can be inferred that substituents which properly stabilize the charge

DOI: 10.1021/jp511057f
J. Phys. Chem. B 2015, 119, 5518−5530

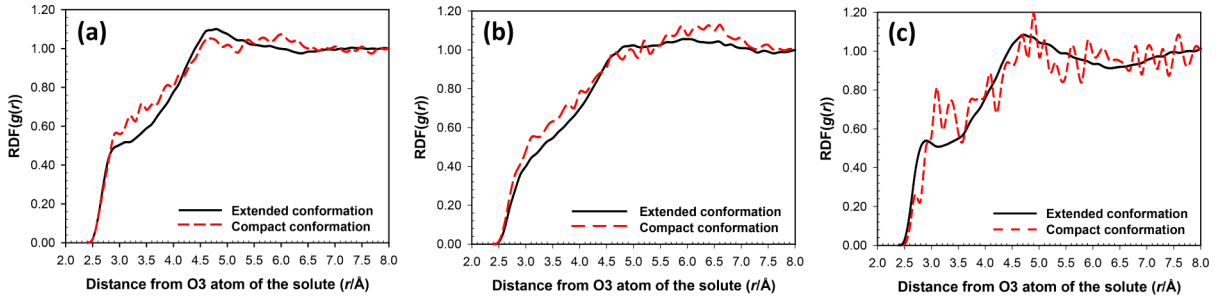

Figure 6. Radial distribution functions (RDFs) of water molecules around the reactant in AVE−water (a), (2-MeO)AVE (b), and (6-MeO)AVE (c) systems, where black solid lines correspond to the extended conformation and red dashed lines to the compact conformation. The O3 atom at each solute was chosen as the center of the RDF.

Table 4. Number of Hydrogen Bonds

	AVE	(2-MeO)AVE	(6-MeO)AVE
compact conformation	0.58(0.12)	0.47(0.07)	0.52(0.08)
extended conformation	0.62(0.01)	0.40(0.03)	0.75(0.01)
Δ(number of hydrogen bonds)	−0.03	0.07	−0.22

redistribution observed in our simulations might shift the equilibrium toward compact conformers. More importantly, the substituent effect will manifest in terms of entropy as well. For instance, (2-MeO)AVE experienced a fairly smaller entropy penalty than parent AVE to adopt the compact conformation in aqueous solution.

We also hoped to look into indirect solvation effects on K_{conf} taking the solvent coordinates into account. In fact, the solid-state structures of BsCM and EcCM[27] provide more clues for understanding the water-acceleration effect: the adjacent, protonated, active site residues exert conformational control in the chorismate mutase E−S complex to lock the ionic substrate in the requisite chairlike conformer for rearrangement. This observation reminds us that, under the aqueous condition, the hydrophobic effect tends to bring close the two apolar moieties in the reactant,[61] and the large cohesive energy of water may prefer those conformers with smaller cavity volumes in aqueous surroundings. According to the total volume changes of the aqueous solutions containing parent and substituted AVEs, when the compact conformers dominate, the solution shrinks concomitantly, and the energy of the whole system decreases. It is noteworthy that this correlation is partially resulted from the energy preference of the solvent itself. If the solute were moved into another solvent with smaller cohesive energy, such an effect would become weaker, as the case in methanol, toluene, etc. In addition, solvents of high cohesive energy density should be in favor of compact conformers. A solvent with cohesive pressure higher than water could serve as a better candidate to reduce ΔG_{conf}, for instance, the ionic liquid.[73]

According to our data (Table 3), it is clear that changing the solvation environment of AVE leads to a reduction of compact conformation population, which is characterized by a positive $\Delta\Delta G_{conf}$. In comparison with the aqueous circumstance, the enthalpy change was the dominant factor that caused AVE to lose a certain preference over compact structures in organic solvents. This is not hard to understand given that neither the intramolecular polarization nor the cohesive energy stabilization is present in these contexts, which in turn corroborates our explanation for the compact conformation accumulation in water.

Given $\Delta\Delta G_{conf}$ of 1−2 kcal/mol, the rate constant at room temperature could be altered by a factor of 20−30.[21] To the best of our knowledge, this is the first computational evidence for hydrophobic effect facilitated Claisen rearrangement, which experimentalists had proposed for decades.[74,75] The substituents will alter the interaction between water and solutes, as well as the entropy changes during structural transformation, resulting in a different population of the compact conformation. From this point of view, it can be inferred that substituents which maintain or increase the hydrophobicity of the solute are expected to cause a rise of the equilibrium constant in water.

III. Interactions between Solute and Water. Accurate quantifying of the interaction between the reactant and solvent remains a challenge, since the interaction energy is usually small while its fluctuation is large. However, we can still manage to gain some insight qualitatively resorting to the radial distribution function (RDF) of water around the solute (Figure 6). From the difference in the RDF around the first-solvation shell (O3−O_w < 4.0 Å, O_w represents oxygen of the water molecule), it can be found that there are more water molecules close to compact conformers, indicating a stronger interaction between water and solutes in compact conformations.

Besides, since the hydrogen bond between O3 atom and solvent was proposed by previous studies to be important during the catalytic activation process,[11] the hydrogen bond numbers in the compact and extended conformations are analyzed (Table 4). In previous theoretical studies on the chorismate, where the carboxyl group is highly hydrophilic, the energy contribution from hydrogen bond formation between the carboxyl group and water was accredited to the solvent effect which changes the diaxial−diequatorial conformational equilibrium.[24,26] However, no significant difference is seen for (2-MeO)AVE and AVE. This finding is in line with the electron population analysis, showing that O3 does not undergo a big change in electron density during conformational transitions. While for 6-methoxy-AVE, which exhibits a distinct pattern of RDF from AVE and (2-MeO)AVE, the result shows that it also suffers more loss of hydrogen bonds than the other two reactants. Therefore, in terms of the solutes like AVEs which are much less hydrophilic than chorismate, the shift of the conformational equilibrium was subjected to different driving

DOI: 10.1021/jp511057f
J. Phys. Chem. B 2015, 119, 5518−5530

forces; at least the direct hydrogen bonding did not seem to be the cause of the stability of compact AVEs in water.

IV. Further Development of SITS-QM/MM MD: Application in Chemical Transitions. All the results and discussion above do not trespass into the electronic configuration space. However, the major barrier of the whole reaction undoubtedly lies in the pathway where the compact reactant transits to the 6-member-ring activated complex. In principle, this process can be monitored using QM/MM MD, but technically, it will be quite difficult if not assisted by IRCs. A large number of computational studies, including QM and QM/MM ones, on the chemical transition event in Claisen rearrangement were carried out, while each of them involved an IRC. In contrast, SITS liberates relevant simulations from IRC. It can be used to sample the chemical transition events if the built-in parameters, including the sampling temperature range and intervals, are finely tuned in order to divert more sampling effort from conformational space onto the chemical configurations. Thus, SITS-QM/MM MD allows us to monitor the occurrence of the bond-rearrangement process of AVE initiated from compact reactants rather than strictly chairlike structures. The results will be presented elsewhere. A relevant paper is in preparation.

CONCLUSION

SITS-integrated QM/MM MD under ambient conditions was carried out to investigate aliphatic Claisen rearrangement in aqueous and nonaqueous solutions. SITS exempted the simulation from IRC, and searched the conformational space of the reactant efficiently. From the simulations, the conformational ensembles of AVEs were obtained, and the structural compact conformation of parent and substituted AVEs was observed and defined. The compact conformers exhibited energetic and electronic features different from extended ones. Assuming that conformational transitions were a lot faster than bond-making/breaking events, a conformational equilibrium between compact and extended structures was proposed prior to the electronic rearrangement in this pericyclic reaction. This subdivision of the reaction coordinate was echoed by the well-documented conformational studies of chorismate mutase.[26,67,76,77] K_{conf} and ΔG_{conf} were calculated to describe the equilibrium. By virtue of the compatibility of SITS over different temperatures, $G-T$ series near 300 K were obtained, and further processed to give rise to ΔH_{conf} and ΔS_{conf}.

The substituent effect was unexceptionally present in ΔG_{conf}, ΔH_{conf}, and particularly in ΔS_{conf}. Substituents altered the solute−solvent interactions, which partly contributed to the varied ΔH_{conf}'s and, more importantly, impacted the entropy penalty during the conformational transition. By and large, the 2-methoxyl substituent did not alter the conformational equilibrium too much in reference of parent AVE, while the 6-methoxyl substituent greatly increased ΔG_{conf} and became unfavorable to adopt the reactive, compact conformation.

In addition, according to the decrease of the partial molar volume of water when the solute transforms to a compact structure, the hydrophobic effect was suggested to create a large impact on ΔH_{conf}, and hence ΔG_{conf}. This result might provide more clues to understanding the "on/in water" acceleration of Claisen rearrangement and other reactions involved with similar hydrophobic reactants.[30,42,62] These features vanish in common organic solvents such as methanol, DMSO, and toluene due to the small CED and the lack of volume shrinkage, ending with an unfavorable enthalpy penalty in the formation of a compact conformer. The recurrence of the compact conformer accumulation in ionic liquid further solidified our conclusion.

Besides, the electron density of the small reactant molecule was found to respond to the conformational changes according to Mulliken population analyses which were available within the QM/MM regime. Also, this could be related to the discovery that the compact conformers were energetically more favorable than the stretched ones in water due to alteration of the charge distribution and the intramolecular polarization. This result showed caveats that conformational changes should be treated carefully even in the case of a small chemical compound.

In order to achieve the thermodynamic data from QM/MM computational simulations more efficiently and systematically, we provide a new enhanced sampling method selectively targeting the QM-treated part. Also, it is compatible in principle with any quantum method. The quantum method in this research, namely, DFTB, which stays at the semiempirical level, is capable of treating small and simple organic compounds such as AVE reasonably in the conformational space. However, the accuracy would be a concern when a bond-forming/breaking event occurred and when heavy atoms were present. Still, one can choose DFT or even higher-level quantum methods available in QM/MM simulations for more accurate research of other demanding processes such as enzymatic reactions and chemical reactions. SITS will promote the efficiency of these multiscale computations as well.

ASSOCIATED CONTENT

Supporting Information

Simulation details and the force field parameters used for constructing nonaqueous solutions are included in SI Text I. A detailed discussion over the convergence of the SITS-MD simulation data was documented in SI Text II and Table S1. The linearity of the $\Delta G_{conf}-T$ plot and nonlinear pattern of the $\Delta G_{conf}/T - T^{-1}$ plot are explained and discussed in SI Text III, and more paradigms for the entropy/enthalpy analyses are shown in Figures S1 and S2. Besides, Figure S3 was drawn to validate the robustness of our method adopted to analyze thermodynamic properties from $\Delta G_{conf}-T$ dependence. The distribution of water under 299 K was additionally shown in Figure S4 as a supplementation to Figure 1 in the main text. In addition, we benchmarked the performance of SCC-DFTB in calculating SCF energy and charge distribution of AVE in SI Text IV and Table S2. The QM SCF energies of AVE in different solvents were included in Table S3, while the electron polarization patterns are shown in Figure S5. Thermodynamic properties of (2-MeO)AVE are listed in Table S4. This material is available free of charge via the Internet at http://pubs.acs.org.

AUTHOR INFORMATION

Corresponding Author

*Phone: +86-10-62752497. E-mail: gaoyq@pku.edu.cn.

Notes

The authors declare no competing financial interest.

ACKNOWLEDGMENTS

We thank the National Program on Key Basic Research Project (973 Programs, No. 2012CB917304) and the Natural Science Foundation of China (91027044, 21125311, and 21373016) for financial support.

DOI: 10.1021/jp511057f
J. Phys. Chem. B 2015, 119, 5518−5530

REFERENCES

(1) Reichardt, C.; Welton, T. *Solvents and Solvent Effects in Organic Chemistry*; John Wiley & Sons: 2011.
(2) McCammon, J. A.; Harvey, S. C. *Dynamics of Proteins and Nucleic Acids*; Cambridge University Press: 1988.
(3) Senn, H. M.; Thiel, W. QM/MM Methods for Biomolecular Systems. *Angew. Chem., Int. Ed.* **2009**, *48*, 1198−1229.
(4) Hu, H.; Yang, W. Free Energies of Chemical Reactions in Solution and in Enzymes with Ab Initio QM/MM Methods. *Annu. Rev. Phys. Chem.* **2008**, *59*, 573.
(5) Guimarães, C. R. W.; Repasky, M. P.; Chandrasekhar, J.; Tirado-Rives, J.; Jorgensen, W. L. Contributions of Conformational Compression and Preferential Transition State Stabilization to the Rate Enhancement by Chorismate Mutase. *J. Am. Chem. Soc.* **2003**, *125*, 6892−6899.
(6) Majumdar, K. C.; Alam, S.; Chattopadhyay, B. Catalysis of the Claisen Rearrangement. *Tetrahedron* **2008**, *64*, 597−643.
(7) Davidson, M. M.; Hillier, I. H.; Hall, R. J.; Burton, N. A. Effect of Solvent on the Claisen Rearrangement of Allyl Vinyl Ether Using Ab Initio Continuum Methods. *J. Am. Chem. Soc.* **1994**, *116*, 9294−9297.
(8) Gao, J. Combined QM/MM Simulation Study of the Claisen Rearrangement of Allyl Vinyl Ether in Aqueous Solution. *J. Am. Chem. Soc.* **1994**, *116*, 1563−1564.
(9) Sehgal, A.; Shao, L.; Gao, J. Transition Structure and Substituent Effects on Aqueous Acceleration of the Claisen Rearrangement. *J. Am. Chem. Soc.* **1995**, *117*, 11337−11340.
(10) Acevedo, O.; Armacost, K. Claisen Rearrangements: Insight into Solvent Effects and "on Water" Reactivity from QM/MM Simulations. *J. Am. Chem. Soc.* **2010**, *132*, 1966−1975.
(11) Severance, D. L.; Jorgensen, W. L. Effects of Hydration on the Claisen Rearrangement of Allyl Vinyl Ether from Computer Simulations. *J. Am. Chem. Soc.* **1992**, *114*, 10966−10968.
(12) Gajewski, J. J. The Claisen Rearrangement. Response to Solvents and Substituents: The Case for Both Hydrophobic and Hydrogen Bond Acceleration in Water and for a Variable Transition State. *Acc. Chem. Res.* **1997**, *30*, 219−225.
(13) Storer, J. W.; Giesen, D. J.; Hawkins, G. D.; Lynch, G. C.; Cramer, C. J.; Truhlar, D. G.; Liotard, D. A. Solvation Modeling in Aqueous and Nonaqueous Solvents. *Structure and Reactivity in Aqueous Solution*; American Chemical Society: Washington, DC, 1994; pp 24−49.
(14) Bartels, C.; Karplus, M. Probability Distributions for Complex Systems: Adaptive Umbrella Sampling of the Potential Energy. *J. Phys. Chem. B* **1998**, *102*, 865−880.
(15) Bussi, G.; Laio, A.; Parrinello, M. Equilibrium Free Energies from Nonequilibrium Metadynamics. *Phys. Rev. Lett.* **2006**, *96*, 090601.
(16) Barducci, A.; Bonomi, M.; Parrinello, M. Metadynamics. *Wiley Interdiscip. Rev.: Comput. Mol. Sci.* **2011**, *1*, 826−843.
(17) Torrie, G. M.; Valleau, J. P. Nonphysical Sampling Distributions in Monte Carlo Free-Energy Estimation: Umbrella Sampling. *J. Comput. Phys.* **1977**, *23*, 187−199.
(18) Yang, L.; Gao, Y. Q. A Selective Integrated Tempering Method. *J. Chem. Phys.* **2009**, *131*, 214109.
(19) Fu, X.; Yang, L.; Gao, Y. Q. Selective Sampling of Transition Paths. *J. Chem. Phys.* **2007**, *127*, 154106.
(20) Chandler, D. Statistical Mechanics of Isomerization Dynamics in Liquids and the Transition State Approximation. *J. Chem. Phys.* **1978**, *68*, 2959−2970.
(21) Hynes, J. T. Chemical Reaction Dynamics in Solution. *Annu. Rev. Phys. Chem.* **1985**, *36*, 573−597.
(22) Mincer, J. S.; Schwartz, S. D. Rate-Promoting Vibrations and Coupled Hydrogen−Electron Transfer Reactions in the Condensed Phase: A Model for Enzymatic Catalysis. *J. Chem. Phys.* **2004**, *120*, 7755−7760.
(23) Daniel, L. S.; William, L. J. Claisen Rearrangement of Allyl Vinyl Ether. *Structure and Reactivity in Aqueous Solution*; American Chemical Society: Washington, DC, 1994; Vol. *568*, pp 243−259.
(24) Martí, S.; Andrés, J.; Moliner, V.; Silla, E.; Tuñón, I.; Bertrán, J. A QM/MM Study of the Conformational Equilibria in the Chorismate Mutase Active Site. The Role of the Enzymatic Deformation Energy Contribution. *J. Phys. Chem. B* **2000**, *104*, 11308−11315.
(25) Martí, S.; Andrés, J.; Moliner, V.; Silla, E.; Tuñón, I.; Bertrán, J. Conformational Equilibrium of Chorismate. A QM/MM Theoretical Study Combining Statistical Simulations and Geometry Optimisations in Gas Phase and in Aqueous Solution. *J. Mol. Struct.: THEOCHEM* **2003**, *632*, 197−206.
(26) Carlson, H. A.; Jorgensen, W. L. Monte Carlo Investigations of Solvent Effects on the Chorismate to Prephenate Rearrangement. *J. Am. Chem. Soc.* **1996**, *118*, 8475−8484.
(27) Lee, A.; Stewart, J. D.; Clardy, J.; Ganem, B. New Insight into the Catalytic Mechanism of Chorismate Mutases from Structural Studies. *Chem. Biol.* **1995**, *2*, 195−203.
(28) Claeyssens, F.; Ranaghan, K. E.; Manby, F. R.; Harvey, J. N.; Mulholland, A. J. Multiple High-Level QM/MM Reaction Paths Demonstrate Transition-State Stabilization in Chorismate Mutase: Correlation of Barrier Height with Transition-State Stabilization. *Chem. Commun.* **2005**, 5068−5070.
(29) Coates, R. M.; Rogers, B. D.; Hobbs, S. J.; Curran, D. P.; Peck, D. R. Synthesis and Claisen Rearrangement of Alkoxyallyl Enol Ethers. Evidence for a Dipolar Transition State. *J. Am. Chem. Soc.* **1987**, *109*, 1160−1170.
(30) Chanda, A.; Fokin, V. V. Organic Synthesis "on Water". *Chem. Rev.* **2009**, *109*, 725−748.
(31) Grieco, P. A. *Organic Synthesis in Water*; Springer: 1998.
(32) Case, D.; Darden, T.; Cheatham, T.; Simmerling, C.; Wang, J.; Duke, R.; Luo, R.; Crowley, M.; Walker, R. C.; Zhang, W. *Amber 10*; University of California: 2008.
(33) Elstner, M.; Porezag, D.; Jungnickel, G.; Elsner, J.; Haugk, M.; Frauenheim, T.; Suhai, S.; Seifert, G. Self-Consistent-Charge Density-Functional Tight-Binding Method for Simulations of Complex Materials Properties. *Phys. Rev. B* **1998**, *58*, 7260.
(34) Han, W. G.; Elstner, M.; Jalkanen, K.; Frauenheim, T.; Suhai, S. Hybrid SCC-DFTB/Molecular Mechanical Studies of H-Bonded Systems and of N-Acetyl-(L-Ala)-Methylamide Helices in Water Solution. *Int. J. Quantum Chem.* **2000**, *78*, 459−479.
(35) Otte, N.; Scholten, M.; Thiel, W. Looking at Self-Consistent-Charge Density Functional Tight Binding from a Semiempirical Perspective. *J. Phys. Chem. A* **2007**, *111*, 5751−5755.
(36) Elstner, M.; Jalkanen, K. J.; Knapp-Mohammady, M.; Frauenheim, T.; Suhai, S. Energetics and Structure of Glycine and Alanine Based Model Peptides: Approximate SCC-DFTB, AM1 and PM3 Methods in Comparison with Dft, Hf and Mp2 Calculations. *Chem. Phys.* **2001**, *263*, 203−219.
(37) Gaus, M.; Cui, Q.; Elstner, M. Density Functional Tight Binding: Application to Organic and Biological Molecules. *Wiley Interdiscip. Rev.: Comput. Mol. Sci.* **2014**, *4*, 49−61.
(38) Seifert, G.; Joswig, J. O. Density-Functional Tight Binding —an Approximate Density-Functional Theory Method. *Wiley Interdiscip. Rev.: Comput. Mol. Sci.* **2012**, *2*, 456−465.
(39) Elstner, M.; Porezag, D.; Jungnickel, G.; Frauenheim, T.; Suhai, S.; Seifert, G. Tight-Binding Approach to Computational Materials Science. *Mater. Res. Soc. Symp. Proc.* **1998**, *491*, 131.
(40) Kumar, A.; Knapp−Mohammady, M.; Mishra, P.; Suhai, S. A Theoretical Study of Structures and Electron Affinities of Radical Anions of Guanine-Cytosine, Adenine-Thymine, and Hypoxanthine-Cytosine Base Pairs. *J. Comput. Chem.* **2004**, *25*, 1047−1059.
(41) Gao, Y. Q. An Integrate-over-Temperature Approach for Enhanced Sampling. *J. Chem. Phys.* **2008**, *128*, 064105.
(42) Gao, Y. Q. Self-Adaptive Enhanced Sampling in the Energy and Trajectory Spaces: Accelerated Thermodynamics and Kinetic Calculations. *J. Chem. Phys.* **2008**, *128*, 134111.
(43) Berendsen, H.; Grigera, J.; Straatsma, T. The Missing Term in Effective Pair Potentials. *J. Phys. Chem.* **1987**, *91*, 6269−6271.
(44) Allen, F. H.; Kennard, O.; Watson, D. G.; Brammer, L.; Orpen, A. G.; Taylor, R. Tables of Bond Lengths Determined by X-Ray and Neutron Diffraction. Part 1. Bond Lengths in Organic Compounds. *J. Chem. Soc., Perkin Trans. 2* **1987**, S1−S19.

DOI: 10.1021/jp511057f
J. Phys. Chem. B 2015, 119, 5518−5530

(45) Frisch, M.; Trucks, G.; Schlegel, H. B.; Scuseria, G.; Robb, M.; Cheeseman, J.; Scalmani, G.; Barone, V.; Mennucci, B.; Petersson, G. *Gaussian 09*, revision A.02; Gaussian, Inc.: Wallingford, CT, 2009.
(46) Bayly, C. I.; Cieplak, P.; Cornell, W.; Kollman, P. A. A Well-Behaved Electrostatic Potential Based Method Using Charge Restraints for Deriving Atomic Charges: The Resp Model. *J. Phys. Chem.* **1993**, *97*, 10269−10280.
(47) Vanquelef, E.; Simon, S.; Marquant, G.; Garcia, E.; Klimerak, G.; Delepine, J. C.; Cieplak, P.; Dupradeau, F.-Y. Red Server: A Web Service for Deriving Resp and Esp Charges and Building Force Field Libraries for New Molecules and Molecular Fragments. *Nucleic Acids Res.* **2011**, *39*, W511−W517.
(48) Dupradeau, F.-Y.; Pigache, A.; Zaffran, T.; Savineau, C.; Lelong, R.; Grivel, N.; Lelong, D.; Rosanski, W.; Cieplak, P. The Red. Tools: Advances in Resp and Esp Charge Derivation and Force Field Library Building. *Phys. Chem. Chem. Phys.* **2010**, *12*, 7821−7839.
(49) Pellegrini, E.; Field, M. J. A Generalized-Born Solvation Model for Macromolecular Hybrid-Potential Calculations. *J. Phys. Chem. A* **2002**, *106*, 1316−1326.
(50) Nam, K.; Gao, J.; York, D. M. An Efficient Linear-Scaling Ewald Method for Long-Range Electrostatic Interactions in Combined QM/MM Calculations. *J. Chem. Theory Comput.* **2005**, *1*, 2−13.
(51) Walker, R. C.; Crowley, M. F.; Case, D. A. The Implementation of a Fast and Accurate QM/MM Potential Method in Amber. *J. Comput. Chem.* **2008**, *29*, 1019−1031.
(52) Seabra, G. d. M.; Walker, R. C.; Elstner, M.; Case, D. A.; Roitberg, A. E. Implementation of the Scc-Dftb Method for Hybrid QM/MM Simulations within the Amber Molecular Dynamics Package. *J. Phys. Chem. A* **2007**, *111*, 5655−5664.
(53) Ryckaert, J.-P.; Ciccotti, G.; Berendsen, H. J. Numerical Integration of the Cartesian Equations of Motion of a System with Constraints: Molecular Dynamics of N-Alkanes. *J. Comput. Phys.* **1977**, *23*, 327−341.
(54) Berendsen, H. J.; Postma, J. P. M.; van Gunsteren, W. F.; DiNola, A.; Haak, J. Molecular Dynamics with Coupling to an External Bath. *J. Chem. Phys.* **1984**, *81*, 3684−3690.
(55) Kurti, L.; Czakó, B. *Strategic Applications of Named Reactions in Organic Synthesis*; Elsevier: 2005.
(56) Yin, Y.; Yang, L.; Zheng, G.; Gu, C.; Yi, C.; He, C.; Gao, Y. Q.; Zhao, X. S. Dynamics of Spontaneous Flipping of a Mismatched Base in DNA Duplex. *Proc. Natl. Acad. Sci. U.S.A.* **2014**, *111*, 8043−8048.
(57) Shao, Q.; Gao, Y. Q. Temperature Dependence of Hydrogen-Bond Stability in B-Hairpin Structures. *J. Chem. Theory Comput.* **2010**, *6*, 3750−3760.
(58) Liu, C.-W.; Wang, F.; Yang, L.; Li, X.-Z.; Zheng, W.-J.; Gao, Y. Q. Stable Salt−Water Cluster Structures Reflect the Delicate Competition between Ion−Water and Water−Water Interactions. *J. Phys. Chem. B* **2014**, *118*, 743−751.
(59) Schuler, F. W.; Murphy, G. W. The Kinetics of the Rearrangement of Vinyl Allyl Ether1. *J. Am. Chem. Soc.* **1950**, *72*, 3155−3159.
(60) Brower, K. R. The Volume Change of Activation in the Claisen and Curtius Rearrangements. *J. Am. Chem. Soc.* **1961**, *83*, 4370−4372.
(61) Chandler, D. Interfaces and the Driving Force of Hydrophobic Assembly. *Nature* **2005**, *437*, 640−647.
(62) Jung, Y.; Marcus, R. On the Theory of Organic Catalysis "on Water". *J. Am. Chem. Soc.* **2007**, *129*, 5492−5502.
(63) Ganem, B. The Mechanism of the Claisen Rearrangement: Déjà Vu All over Again. *Angew. Chem., Int. Ed. Engl.* **1996**, *35*, 936−945.
(64) Copley, S. D.; Knowles, J. R. The Conformational Equilibrium of Chorismate in Solution: Implications for the Mechanism of the Non-Enzymic and the Enzyme-Catalyzed Rearrangement of Chorismate to Prephenate. *J. Am. Chem. Soc.* **1987**, *109*, 5008−5013.
(65) Hur, S.; Bruice, T. C. The near Attack Conformation Approach to the Study of the Chorismate to Prephenate Reaction. *Proc. Natl. Acad. Sci. U.S.A.* **2003**, *100*, 12015−12020.
(66) Guo, H.; Cui, Q.; Lipscomb, W. N.; Karplus, M. Substrate Conformational Transitions in the Active Site of Chorismate Mutase: Their Role in the Catalytic Mechanism. *Proc. Natl. Acad. Sci. U.S.A.* **2001**, *98*, 9032−9037.
(67) Campbell, A. P.; Tarasow, T. M.; Massefski, W.; Wright, P. E.; Hilvert, D. Binding of a High-Energy Substrate Conformer in Antibody Catalysis. *Proc. Natl. Acad. Sci. U.S.A.* **1993**, *90*, 8663−8667.
(68) Burrows, C. J.; Carpenter, B. K. Substituent Effects on the Aliphatic Claisen Rearrangement. 1. Synthesis and Rearrangement of Cyano-Substituted Allyl Vinyl Ethers. *J. Am. Chem. Soc.* **1981**, *103*, 6983−6984.
(69) Bolhuis, P. G.; Chandler, D.; Dellago, C.; Geissler, P. L. Transition Path Sampling: Throwing Ropes over Rough Mountain Passes, in the Dark. *Annu. Rev. Phys. Chem.* **2002**, *53*, 291−318.
(70) Gajewski, J. J.; Jurayj, J.; Kimbrough, D. R.; Gande, M. E.; Ganem, B.; Carpenter, B. K. The Mechanism of Rearrangement of Chorismic Acid and Related Compounds. *J. Am. Chem. Soc.* **1987**, *109*, 1170−1186.
(71) Rhoads, S. J.; Raulins, N. R. The Claisen and Cope Rearrangements. *Org. React.* **1975**, *22*, 1−252.
(72) Brandes, E.; Grieco, P.; Gajewski, J. Effect of Polar Solvents on the Rates of Claisen Rearrangements: Assessment of Ionic Character. *J. Org. Chem.* **1989**, *54*, 515−516.
(73) Gajewski, J. J. A Semitheoretical Multiparameter Approach to Correlate Solvent Effects on Reactions and Equilibria. *J. Org. Chem.* **1992**, *57*, 5500−5506.
(74) Joseph, J. G.; Nancy, L. B. Factor Analysis of Solvent Effects on Reactions. *Structure and Reactivity in Aqueous Solution*; American Chemical Society: Washington, DC, 1994; Vol. *568*, pp 229−242.
(75) Lubineau, A.; Augé, J.; Bellanger, N.; Caillebourdin, S. Water-Promoted Organic Synthesis Using Glyco-Organic Substrates: The Claisen Rearrangement. *J. Chem. Soc., Perkin Trans. 1* **1992**, 1631−1636.
(76) Khanjin, N. A.; Snyder, J. P.; Menger, F. Mechanism of Chorismate Mutase: Contribution of Conformational Restriction to Catalysis in the Claisen Rearrangement. *J. Am. Chem. Soc.* **1999**, *121*, 11831−11846.
(77) Xue, Y.; Lipscomb, W. N. Location of the Active Site of Allosteric Chorismate Mutase from Saccharomyces Cerevisiae, and Comments on the Catalytic and Regulatory Mechanisms. *Proc. Natl. Acad. Sci. U.S.A.* **1995**, *92*, 10595−10598.

DOI: 10.1021/jp511057f
J. Phys. Chem. B 2015, 119, 5518−5530